Initial development of an industrial tool to model water atomization of metals

Ali Asgarian[1,2,*], Robert Alicandri[1], Markus Bussmann[2], Kinnor Chattopadhyay[1]
[1] Department of Materials Science & Engineering, University of Toronto, 184 College Street, Toronto, Ontario, Canada M5S 3E4
[2] Department of Mechanical and Industrial Engineering, University of Toronto, 5 King's College Road, Toronto, Ontario, Canada M5S 3G8

ABSTRACT: A combined physical-numerical modelling approach has been used to analyze flat-fan water sprays common in water atomization of metals, where a molten metal stream is impinged by a number of high-pressure water sprays. Due to the energy transfer at the impingement zone, the molten metal stream breaks up into droplets that ultimately become powder. In this study, a lab-scale setup was built to carry out high-speed imaging of a high-pressure, low flowrate spray. Digitally-analyzed shadowgraphs were used to determine the characteristics of the flat-fan spray, acting as inputs for predictive modelling of water spray droplet formation after primary breakup, using previous models in the literature. The spray droplet diameter after primary breakup was calculated numerically and compared with experimental measurements. A good agreement exists between experimental, theoretical, and previously-published numerical results after accounting for thinning of the liquid sheet due to radial divergence of the fan. The initial development of an industrial tool for predicting water droplet size is presented, with more features to be included in the future.

Key words:
Water Atomization
Metal Powder
High Speed Imaging
Numerical Modelling
Droplet Size

1. Introduction

Powder metallurgy (PM) is a growing technology for producing net-shape (or near net-shape) metal parts from powdered metal. PM techniques offer flexibility in component design while reducing energy and material consumption [1]. With recent advances, PM has become a competitive production method for high-quality and high-strength parts. As a means of further advancing the field, many researchers have studied the effects of metal powder characteristics on the quality of final products. However, little effort has been devoted to the upstream processes to identify the relationships between powder metal

*Corresponding author.
Email address:ali.asgarian@utoronto.ca (A. Asgarian).

Received DD MM YYYY; Received in revised form DD MM YYYY; Accepted DD MM YYYY
Available online DD MM YYYY

characteristics and the operating and design parameters of powder production processes, the most economical one being water atomization of molten metals. Water atomization, which is the subject of the present study, is the main route for high volume metal powder production [2]. As Pasupathy et al. [3] note, there are seldom few quantitative descriptions of how powder characteristics, including median particle size, particle size distribution, and particle shape, relate to a given set of operating/design parameters, e.g. water spray nozzle design, water pressure, and molten metal properties. Among powder characteristics, the median particle size is the most studied feature for which a number of empirical or semi-empirical equations have been proposed ([4 -7]). While these equations relate the median particle size to operating parameters, they only provide reliable results for specific water atomizer setups and molten metal properties. Therefore, these equations cannot reliably be generalized to other operational setups. To respond to this knowledge gap, Asgarian et al. [8,9] quantitatively studied the first and most important part of the water atomization process—the water spray. They highlight the idea that spray features, e.g. droplet size distribution, affect the as-atomized powder characteristics, e.g. powder size distribution. Building on this hypothesis, they simulated flat-fan sprays, commonly used in the water atomization process, using computational fluid dynamics (CFD). In addition, they validated the CFD results by means of high-speed imaging of the water sprays. While CFD is a versatile simulation tool, it requires considerable background knowledge and preparation to both utilize and validate the simulation results. In addition, accessibility to CFD as a design tool is limited due to the cost of commercial software licenses. Therefore, in this present work, we present a more accessible and industrially-suitable calculation tool, incorporating advanced theory, that provides a reasonable estimate of droplet size for flat-fan sprays for metal powder manufacturers.

2. Experimental Procedure

The experimental setup used in [8,9] was also used for the present study. A schematic and a photograph of the experimental setup are shown in Fig. 1. A high-speed camera and a back light were used to image the spray shadow (shadowgraph). The shadowgraphs were then post-processed using ImageJ, an open-source image processing software, to obtain the required input data for spreadsheet calculation. The input parameters include the spray spreading angle β, the breakup length B_L, and the water sheet width T_W at the nozzle exit, which are depicted in Fig. 3 and 5.

The flat-fan nozzle specifications are listed in Table 1, and photos of the nozzle are shown in Fig. 2. As shown in Fig. 2, the orifice geometry of the nozzle corresponds to the intersection of a transverse curved slit and a hemisphere at the end of the internal passage. This results in an elliptical orifice with large and small diameters of about 1.77 mm and 0.97 mm, respectively. In the present study, experimental and numerical results of a spray at 2068 kPa (300 psi) will be presented.

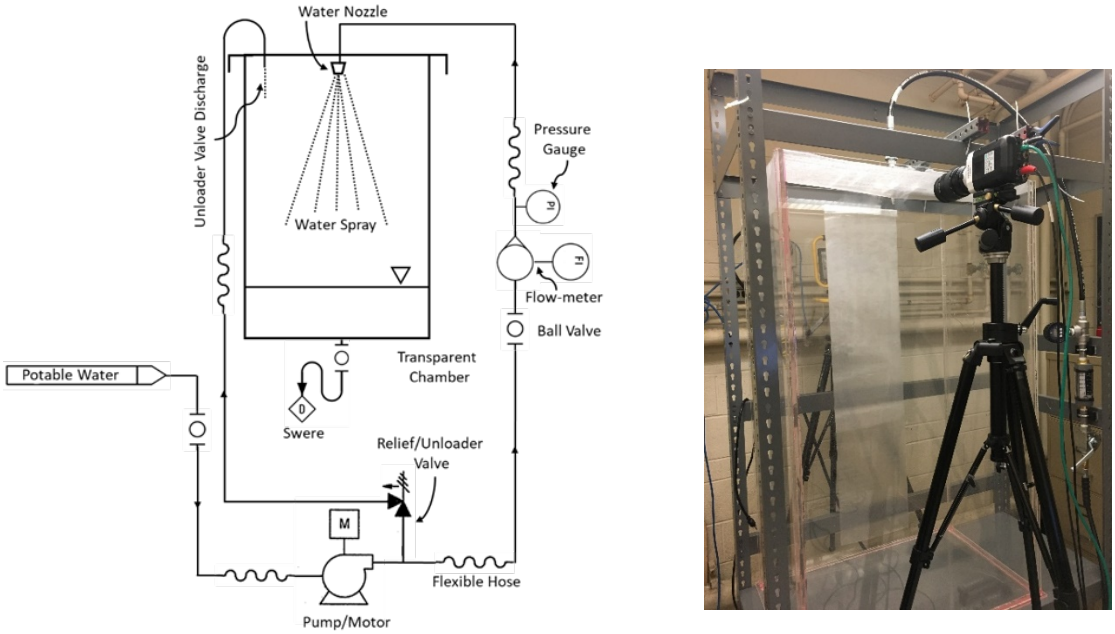

(a) (b)

Fig. 1 (a) Flow diagram and (b) photo of the experimental setup

(a) (b)

Fig. 2 Flat-fan spray nozzle (a) side view (b) cross section

Table 1

Nozzle specifications

Nozzle type	Hydraulic diameter, D_h (mm)	Flowrate at 2068 kPa (300 psi) (L/min)	Flowrate at 10,000 kPa (1450 psi) (L/min)	Spreading angle (°)*
Flat-Fan Spray	1.16	4.16	9.1	25

* This is a vendor published value; however, the spreading angle varies with pressure.

3. Numerical Model

The numerical model utilized in this study is that proposed by Senecal et al. [10], where the breakup of a 2D viscous liquid sheet is caused by periodic disturbances. Breakup occurs as a staged process where an initial disturbance, be it aerodynamic drag or internal turbulence, is amplified, leading to the formation of cylindrical ligaments, which then break into droplets by means of transverse waves. Based on the linear instability analysis of Dombrowski and Johns [11], the breakup of the sheet into ligaments transitions from long-wave dominated to short-wave dominated at a critical gas Weber number, We_g, of 27/16. For the 2068 kPa (300 psi) spray case analyzed in this work, it is initially assumed that We_g exceeds this critical

value, and so ligament formation will be short-wave dominated. This assumption is verified by back-calculation with the half-sheet thickness, h, estimated as described later in this section. The back-calculation is shown in Equation 1 below. Note that all equation parameters are defined in Table 2 at the end of this section.

$$We_g = \frac{\rho_2 V^2 h}{\sigma} = \frac{1.1839\ \frac{kg}{m^3}\left(59.12\frac{m}{s}\right)^2 \cdot 54.55 \cdot 10^{-5}\ m}{0.07199\ \frac{N}{m}} = 3.14 > \frac{27}{16} \quad (1)$$

In the case of short-wave dominated sheet breakup, Equation 2 (equation 33 in [10]) relates the wave growth rate, ω_t, to the wave number, k, of the initial sheet disturbance, and various physical and process properties of the sheet including water viscosity and surface tension:

$$\omega_t = -2\nu_1 k^2 + \sqrt{4\nu_1^2 k^4 + QV^2 k^2 - \frac{\sigma k^3}{\rho_1}} \quad (2)$$

The formation of ligaments due to sheet breakup is predicted to occur at the maximal wave growth rate, Ω_s, occurring within the sheet. The corresponding ligament diameter, d_L, is then a function of the most unstable wave number, K_S, and sheet half thickness at breakup, h, as described in Equation 3 (equation 39 in [10]), where K_S is obtained by maximizing ω_t in Equation 2:

$$d_L = \sqrt{\frac{16h}{K_s}} \quad (3)$$

Following the further analysis of Senecal et al. [10], based on the breakup of a cylindrical viscous column [12], the diameter of a water droplet, d_D , after primary breakup can be estimated as a function of ligament diameter and the liquid properties, as shown in Equation (4) (equation 41 of [7]):

$$d_D = 1.88 d_L \left(1 + \frac{3\mu_1}{\sqrt{\rho_1 \sigma d_L}}\right)^{1/6} \quad (4)$$

The primary contribution of the present work is to present a model of droplet size that has been implemented in an industrially-friendly tool, and that incorporates insights from recently-completed shadowgraph imaging. In this manner, K_S in Equation (3) is calculated by numerically maximizing Equation (2) by analyzing for a sign change in the first derivative over an interval bounded between 0 and the length-normalized Weber number. The half-sheet thickness parameter, h, of Equations (1) and (3) is calculated by applying continuity of mass to the flat-fan spray, where widening of the spray with distance from the nozzle tip implies overall sheet thinning up to the point of sheet breakup. Assuming sheet velocity does not vary significantly with increasing distance from the nozzle tip, the cross-sectional area of the spray perpendicular to the flow must remain constant. This leads to the equality shown in Equation (5) below. Values for sheet width and thickness at the nozzle tip, T_w and T_t respectively, were measured by digital image analysis as demonstrated in Fig. 4, while the breakup width, B_W, is calculated geometrically from the spreading angle, β, and the breakup length, B_L, as shown in Fig. 3:

$$B_w \cdot 2h = T_w T_t \rightarrow h = \frac{T_w T_t}{2B_w},$$

$$h = \frac{T_w T_t}{2[2B_L \tan\left(\frac{\beta}{2}\right) + T_w]},$$

$$h = \frac{T_w T_t}{\frac{48V}{\Omega_s} tan\left(\frac{\beta}{2}\right) + 2T_w} \quad (5)$$

The breakup length is calculated using Equation 6 (equation 35 in [10]) with the sheet velocity and previously calculated Ω_s parameter used as input:

$$B_L = \frac{12\ V}{\Omega_s} \tag{6}$$

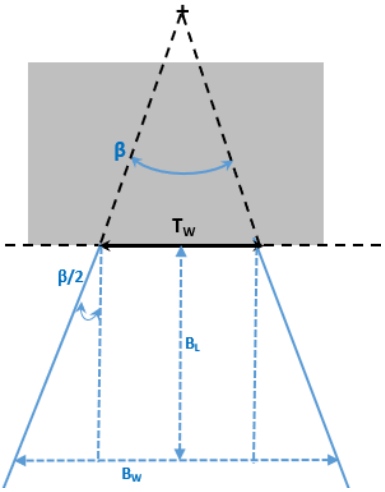

Fig. 3 Schematic of the geometric layout for calculation of half-sheet thickness at point of breakup

Future work will extend the numerical model to the case of long-wave dominant ligament formation, as well as incorporate the effect of varying sheet velocity as a function of distance from the nozzle tip at the point of sheet breakup.

Table 2

Equation parameters utilized in this study

Symbol	Meaning	Value	Units
h	Half-sheet thickness at point of breakup	66.19	μm
ρ_1	Density of water at 25°C	997.0	kg/m^3
ρ_2	Density of air at 25°C	1.1839	kg/m^3
μ_1	Dynamic viscosity of water at 25°C	$8.90 \cdot 10^{-4}$	Pa·s
ν_1	Kinematic viscosity of water at 25°C	$8.93 \cdot 10^{-7}$	m^2/s
σ	Surface tension of water	0.072	N/m
Q	Ratio of air to water density (ρ_2/ρ_1)	0.0012	--
V	Sheet velocity*	59.12	m/s
P	Spray Pressure	2068	kPa
k	Wave number	--	1/m
K_s	Most unstable wave number	36919	1/m
ω_t	Wave growth rate	--	1/s
Ω_s	Maximal wave growth rate	42624	1/s
B_L	Calculated breakup length relative to nozzle tip	16.64	mm
B_W	Width of fan at the breakup length	15.39	mm
β	Spray spreading angle	39.8	°
T_w	Measured sheet width at the nozzle tip	3.58	mm
T_t	Measured sheet thickness at the nozzle tip	0.62	mm
d_L	Calculated ligament diameter	171.2	μm
d_D	Calculated droplet diameter	323.1	μm

* Sheet velocity estimated from spray pressure P by $V = 1.3\sqrt{P}$

3. Results and Discussion

The spray was visualized from the front and side (see Fig. 4). The liquid sheet is observed immediately at the outlet of the nozzle; however, shortly after it breaks up into transverse ligaments.

As shown in Fig. 4(a), the sheet breakup occurs within 2 cm of the nozzle exit. The numerically-calculated breakup length of 1.66 cm is in good agreement with this observation.

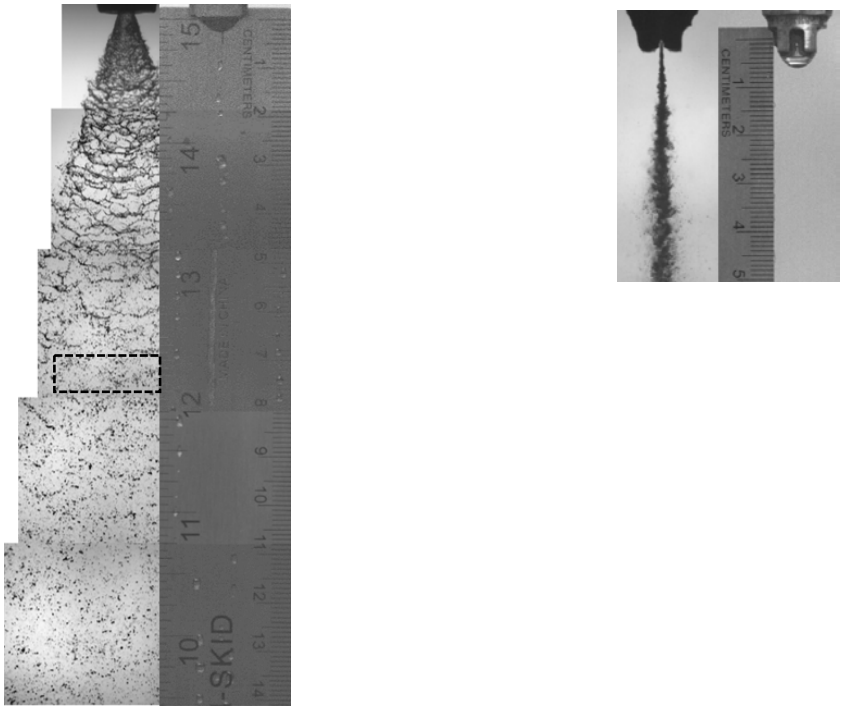

(a) Front (b) Side

Fig. 4 Shadowgraphs of the 2068 kPa (300 psi) water spray (a) front view and (b) side view.

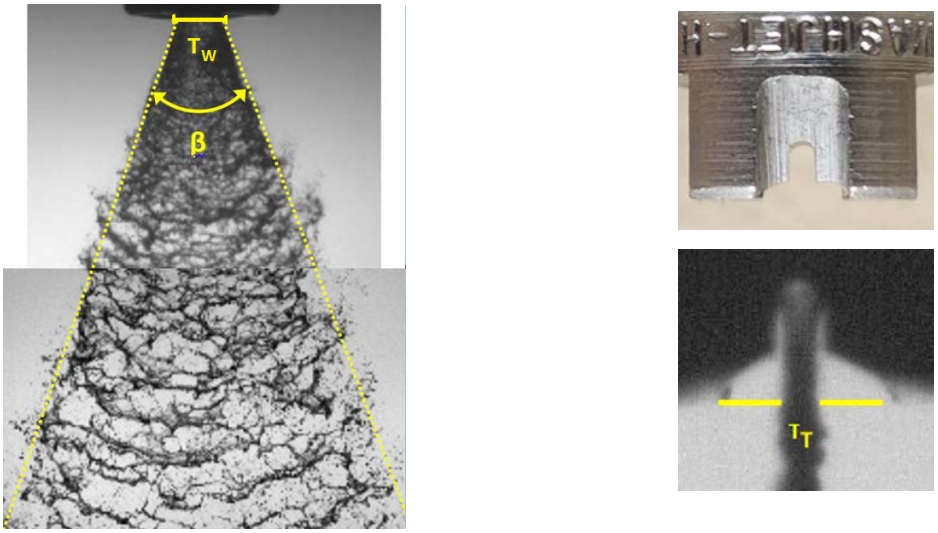

(a) Front (b) Side

Fig. 5 (a) Spray spreading angle β = 39.8° and fan width at the nozzle tip T_W = 3.36mm measured from the front view, and (b) fan thickness at the nozzle tip T_T = 0.62mm measured from the side view

It can be seen in Fig. 5(b) that air surrounds the liquid stream inside the nozzle slit, resulting in a sheet thinner than the slit.

Although sheet breakup occurs at approximately 2 cm from the nozzle tip, the disintegration of ligaments into droplets is a gradual process and is incomplete up to a distance of nearly 7 cm below the nozzle. Therefore, the droplet size measurement was done in the region of 7.5-8 cm below the nozzle (the dashed box in Fig. 4(a). The steps of image processing are shown in Fig. 6(b).

There are different definitions for droplet mean diameter in the literature; however, the one that is commonly used for comparison with the result of primary breakup theory is volume mean diameter [13]. The droplet volume mean diameter, D_{30}, is the droplet diameter of a uniform equivalent set with the same number of drops and the same total volume of all drops as the real set. The volume mean diameter obtained from the experiment is D_{30} = 295 μm which is 9 percent smaller than the droplet size of 323.1 μm calculated from primary breakup theory.

The difference between the experimental volume mean diameter and the calculated droplet size can be explained by noting that the disintegration of the ligaments into initial droplets is gradual with no clear boundary existing between primary and secondary breakup of droplets, and it is impractical to verify that the sampled droplets have only undergone primary breakup.

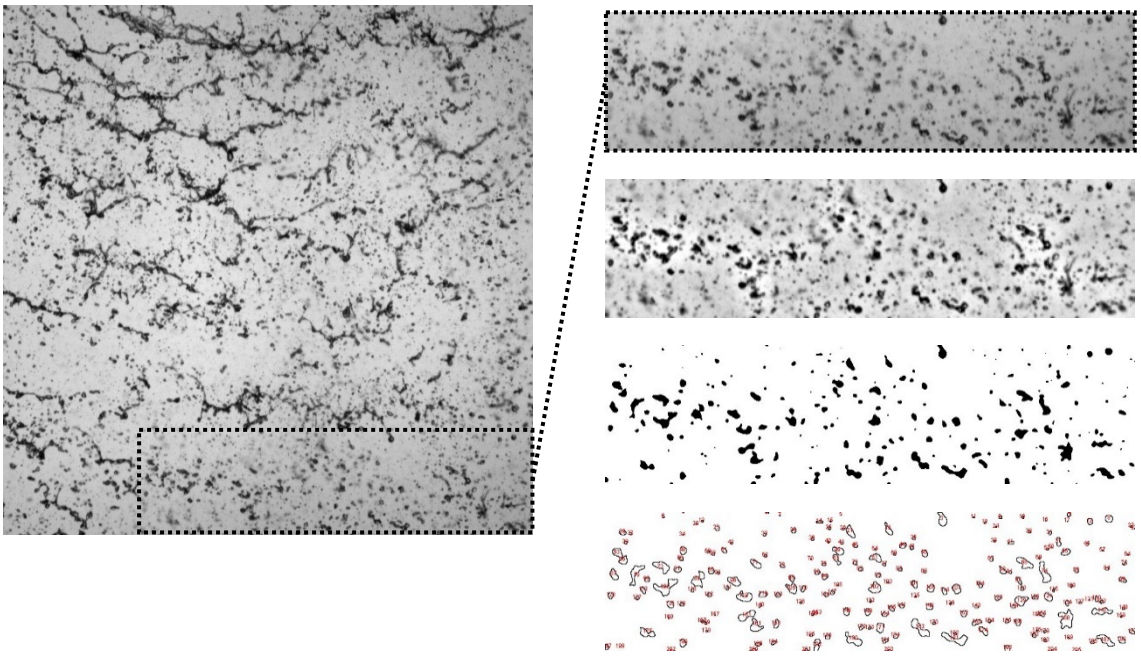

(a) 5 to 8 cm (b) 7.5 to 8 cm

Fig. 6 (a) Shadowgraph of the 2,068 kPa (300 psi) water spray from 5 to 8 cm below the nozzle; the dashed region is 7.5 to 8 cm below the nozzle; (b) Image processing steps, from top to bottom, cropping, FFT filtering, thresholding, and droplet sizing.

4. Conclusions

(1) An experimental flat-fan spray has been imaged and digitally-analyzed to determine a mean droplet size for an operating pressure of 2068 kPa (300 psi).

(2) A numerical tool has been developed using primary breakup theory to estimate the droplet diameter for a flat-fan spray for industrial use if sufficient operational and geometric data is provided.

(3) There is a good agreement between the calculated droplet size and the experimental mean volume diameter (9.5 % deviation). The insignificant difference is believed to be due to the inability to differentiate between droplets that have only undergone primary breakup and those that have also undergone secondary breakup.

(4) Future work includes improving the lighting for the experimental fan spray for greater shadowgraph clarity, and extending the numerical model for long-wave dominated sheet breakup.

Acknowledgments

The authors would like to thank the Natural Sciences and Engineering Research Council of Canada (NSERC) and Rio Tinto Metal Powders for funding this research.

References

[1] Metal Powder Industries Federation (n.d.) Powder Metallurgy—Intrinsically Sustainable. Retrieved February 01, 2018, from https://www.mpif.org/IntroPM/PDFs/PM-Intrinsically-Sustainable.pdf

[2] Neikov, O. D., Nabojchenko, S. S., Murashova, I. B., Gopienko, V. G., Frishberg, I. V., & Lotsko, D. V. (2009). Handbook of non-ferrous metal powders. Technologies and applications by OD Neikov.

[3] Pasupathy, M., Martin, J. M., Iturriza, I., & Castro, F. Effect of the atomizer geometrical configuration on the particle size and shape of water atomized powders. In Proceedings of EURO PM 2011 Powder Metallurgy Congress and Exhibition (pp. 9-14).

[4] Grandzol, R. J., & Tallmadge, J. A. (1975). Effect of jet angle on water atomization. International Journal of Powder Metallurgy & Powder Technology, 11, 103-109.

[5] Dunkley, J. J., & Palmer, J. D. (1986). Factors affecting particle size of atomized metal powders. Powder Metallurgy, 29(4), 287-290.

[6] Bergquist, B. (1999). New insights into influencing variables of water atomisation of iron. Powder Metallurgy, 42(4), 331-343.

[7] Persson, F., Eliasson, A., & Jönsson, P. (2012). Prediction of particle size for water atomised metal powders: parameter study. Powder Metallurgy, 55(1), 45-53.

[8] Asgarian, A., Wu, C., Li, D., Bussmann, M., Chattopadhyay, K., Lemieux, S., Girard, B., Lavallee, F., & Paserin, V. (2018). Experimental and Computational Analysis of a Water Spray; Application to Molten Metal Atomization. To be published in Advances in Powder Metallurgy & Particulate Materials.

[9] Asgarian, A., Heinrich, M., Chattopadhyay, K., & Bussmann, M. (2018). Computational Modelling of Water Sprays in Molten Metal Atomization Process. To be published in Euro PM2018 Congress Proceedings.

[10] Senecal, P. K., Schmidt, D. P., Nouar, I., Rutland, C. J., Reitz, R. D., & Corradini, M. L. (1999). Modeling high-speed viscous liquid sheet atomization. International Journal of Multiphase Flow, 25(6-7), 1073-1097.

[11] N. Dombrowski and W. Johns, "The aerodynamic instability and disintegration of viscous liquid sheets", Chemical Engineering Science, vol. 18, no. 3, pp. 203-214, 1963.
[12] Weber, C., 1931. On the breakdown of a fluid jet. Z.A.M.P 11, 136-159.
[13] Kashani, A., Parizi, H., & Mertins, K. H. (2018). Multi-step spray modelling of a flat fan atomizer. Computers and Electronics in Agriculture, 144, 58-70.